Copy 232
RM L57D04a

NACA

RESEARCH MEMORANDUM

MEASUREMENTS OF HEAT TRANSFER AND BOUNDARY-LAYER TRANSITION ON AN 8-INCH-DIAMETER HEMISPHERE-CYLINDER IN FREE FLIGHT FOR A MACH NUMBER RANGE OF 2.00 TO 3.88

By Benjamine J. Garland and Leo T. Chauvin

Langley Aeronautical Laboratory
Langley Field, Va.

NATIONAL ADVISORY COMMITTEE
FOR AERONAUTICS

WASHINGTON

April 18, 1957

NACA RM L57D04a

NATIONAL ADVISORY COMMITTEE FOR AERONAUTICS

RESEARCH MEMORANDUM

MEASUREMENTS OF HEAT TRANSFER AND BOUNDARY-LAYER TRANSITION ON AN 8-INCH-DIAMETER HEMISPHERE-CYLINDER IN FREE FLIGHT FOR A MACH NUMBER RANGE OF 2.00 TO 3.88

By Benjamine J. Garland and Leo T. Chauvin

SUMMARY

Measurements of aerodynamic heat transfer have been made along the hemisphere and cylinder of a hemisphere-cylinder rocket-propelled model in free flight up to a Mach number of 3.88. The test Reynolds number based on free-stream condition and diameter of model covered a range from 2.69×10^6 to 11.70×10^6.

Laminar, transitional, and turbulent heat-transfer coefficients were obtained. The laminar data along the body agreed with laminar theory for blunt bodies whereas the turbulent data along the cylinder were consistently lower than that predicted by the turbulent theory for a flat plate. Measurements of heat transfer at the stagnation point were, in general, lower than the theory for stagnation-point heat transfer. When the Reynolds number to the junction of the hemisphere-cylinder was greater than 6×10^6, the transitional Reynolds number varied from 0.8×10^6 to 3.0×10^6; however, when the Reynolds number to the junction was less than 6×10^6, the transitional Reynolds number varied from 7.0×10^6 to 24.7×10^6.

INTRODUCTION

Sharp-nose bodies are desirable for use at supersonic speeds because of their known aerodynamic characteristics. However, as the Mach number increases, the aerodynamic heating being a function of the Mach number becomes increasingly severe. Theory shows that the heat-transfer rate at

the nose tip is a function of Mach number and reduces with increasing nose-tip diameter. In order to reduce the heating rates to a tolerable level, the tip diameter must be increased; thereby the aerodynamic characteristics of the sharp tip are compromised. This means of reducing the heat-transfer rates will probably be satisfactory for a large number of flight conditions; however, for other cases, new materials and artificial cooling methods will be required in addition to blunting.

As part of a general program being carried out by the National Advisory Committee for Aeronautics to investigate the effects of shape on the aerodynamic heat transfer and boundary-layer transition, the Langley Pilotless Aircraft Research Division (PARD) has conducted tests to evaluate these properties for various blunt-nose shapes, some of which have been reported in references 1 and 2.

The purpose of the present investigation was to investigate the heat transfer and location of boundary-layer transition on a hemisphere-cylinder at Mach numbers up to 3.88. This was accomplished by telemetering skin-temperature measurements along the hemisphere and cylinder of a two-stage rocket-propelled model. Laminar, turbulent, and transitional heat-transfer data were measured during the test for free-stream Reynolds numbers per foot up to 18.9×10^6. The measured heat-transfer data are compared with existing heat-transfer theories for stagnation-point heat transfer (ref. 3), with the theory of Stine and Wanlass for laminar flow along the hemisphere (ref. 4), and with the theories of Van Driest for laminar and turbulent flow on a flat plate (refs. 5 and 6).

The flight test was conducted at the Langley Pilotless Aircraft Research Station at Wallops Island, Va.

SYMBOLS

b	length from stagnation point to hemisphere-cylinder junction, $\pi D/4$, in.
c_f	local skin-friction coefficient
c_p	specific heat of air, Btu/slug-$^\circ$F
$c_{p,w}$	specific heat of wall material, Btu/lb-$^\circ$F
D	diameter of model, in.
h	aerodynamic heat-transfer coefficient, Btu/(sec)(sq ft)($^\circ$F)
l	distance from stagnation point along surface at model, in.

k	thermal conductivity of air, Btu/(sec)(sq ft)($^{\circ}$F/ft)
M	Mach number
N_{Nu}	Nusselt number, $h(l/12)/k$
N_{St}	Stanton number, $h/c_p\rho V$
N_{Pr}	Prandtl number, $c_p\mu/k$
p	pressure, lb/sq ft
R	Reynolds number, $\rho V(l/12)/\mu$
$R_{\infty,T}$	Reynolds number at transition point, based on free-stream conditions
R_θ	Reynolds number based on laminar-boundary-layer momentum thickness
η_r	recovery factor
T	temperature, $^{\circ}$R unless otherwise indicated
t	time, sec
V	velocity, ft/sec
V_c	velocity of sound, ft/sec
x	distance from stagnation point along axis of model, in.
β	velocity gradient at stagnation point
θ	angle between stations on hemisphere and stagnation point, deg
μ	viscosity of air, slugs/ft-sec
ρ	density of air, slugs/cu ft
ρ_w	specific weight of wall material, lb/cu ft
τ_w	wall thickness, ft

Subscripts:

aw	adiabatic wall
t	isentropic stagnation
l	just outside boundary layer
w	wall (skin) material
∞	undisturbed free stream

MODEL, INSTRUMENTATION, AND TEST

Model

The general model arrangement and pertinent dimensions of the test vehicle are shown in the sketch of figure 1 and in the photograph of figure 2. The body was an 8-inch-diameter hemisphere-cylinder of fineness ratio 17.25 stabilized by three tapered trapezoidal magnesium fins equally spaced. Details of the fins are given in figure 1.

The test vehicle was all metal in construction with spun Inconel being utilized for the nose section, which comprised 20.5 percent of the body length. The rear section was formed from magnesium-alloy skin and a cast-magnesium-alloy tail section to which the fins were welded. Skin thicknesses for each measurement station are shown in table I. All the surfaces were polished and the surface roughness as measured by a Physicists' Research Co. Profilometer was 25 microinches and 60 microinches root mean square for the Inconel and magnesium skin, respectively.

The model was boosted by an M5 JATO rocket motor and the sustainer motor was an ABL Deacon rocket motor. A photograph of the model and booster on the launcher is shown in figure 3.

Instrumentation

The model was equipped with four channels of telemetering, two of which transmitted wall temperatures and the other two, longitudinal acceleration to a ground receiving station. The temperature channel was commutated about every 0.2 second to transmit temperature measurements at the locations shown in table I. Thermocouples 1 to 12 were installed in the Inconel nose section by fusing the thermocouple wire to the inner surface of the skin. Because the rear section of the model was magnesium,

the thermocouple wire could not be fused to the inner skin. The installation was accomplished by placing the bead (the fused junction of the thermocouple wires) into a countersunk hole equal in depth to the skin thickness, filling the hole with molten magnesium, and refinishing the surface to a prescribed finish. The accuracy of the temperatures recorded was within $\pm 15^{\circ}$ F. This value is based on a maximum probable error of ± 2 percent of the calibrated full-scale range, which is the usual accuracy of the PARD flight-model instrumentation. A more complete discussion of the general methods of the temperature telemetering techniques employed is presented in reference 7.

In addition to the instrumentation carried internally, the model was tracked by a CW Doppler radar set and an NACA modified SCR 584 radar set. The former provides the velocity of the model and the latter provides trajectory data. Atmospheric and wind conditions are determined by means of radiosondes launched near the time of flight and tracked by a Rawin set AN/GMD-1A. The model exceeded the range of the CW Doppler radar set, and the velocity data were extended by integration of the telemetered acceleration.

Test

The model was launched from an elevation angle of 75°. The booster accelerated the model to a Mach number of 3.05 where it separated from the model shortly after burnout. The model coasted upwards for a predetermined time until the sustainer rocket motor ignited and accelerated the model to a Mach number of 3.88. This method of flight programming provided large change of Reynolds number for a given Mach number. For example, at the end of the first-stage burnout (M = 3.05), the free-stream Reynolds number per foot is about 19×10^6; whereas, for the same Mach number during the second-stage firing and coasting, the Reynolds numbers are approximately 9×10^6 and 7×10^6, respectively. These and other test conditions will be discussed in greater detail subsequently.

DATA REDUCTION

From the flight test of the model, the following basic information was obtained as a function of time:

(1) Wall-temperature measurements given in figure 4 for thermocouples 1 to 23, the locations of which are listed in table I

(2) Air properties (density, speed of sound, static temperature, and pressure) at any given time (fig. 5)

(3) Free-stream Mach number and Reynolds number per foot (fig. 6)

From these measurements, heat-transfer information was reduced to Stanton number where

$$N_{St}\left(c_p\rho V\right)_l = \frac{c_{p,w}\rho_w T_w \frac{dT}{dt}}{T_{aw} - T_w}$$

Local conditions were obtained from pressure distribution for a hemisphere-cylinder given in references 8 to 10 and from supersonic flow relations for normal shocks.

The adiabatic-wall temperature T_{aw} was obtained from the definition of recovery factor where

$$\eta_r = \frac{T_{aw} - T_l}{T_t - T_l}$$

This relation leads to

$$T_{aw} = T_l + \eta_r\left(T_t - T_l\right)$$

The data along the hemisphere were reduced by using a recovery factor equal to $\left(N_{Pr}\right)^{1/3}$ for turbulent flow and $\left(N_{Pr}\right)^{1/2}$ for laminar flow where the Prandtl number was based on measured wall temperature. For the stagnation point, a recovery factor equal to 1 was used. The thermodynamic properties of air (ρ, N_{Pr}, and so forth) used in the computation were obtained from reference 11.

Properties of the material used in the construction of the model were obtained from reference 12 for the Inconel nose-section and from reference 13 for the magnesium rear section. Skin thicknesses for the various thermocouple locations are given in table I.

Radiation and conduction along the body were evaluated for the times at which data were obtained and were found to be less than 2 percent of the heat due to convection for the worst condition (low values of heat flux $T_{aw} - T_w$).

RESULTS AND DISCUSSION

Local heat-transfer coefficients expressed in the form of Stanton number were reduced from the wall-temperature time histories as described in the section entitled "Data Reduction." Stanton numbers were obtained for various times during the flight as indicated by ticks in figure 6 on the Mach number time history. As can be seen in figure 6, Stanton numbers were obtained for several Reynolds number conditions at each Mach number.

Heat-transfer results are presented in figure 7 for all stations along the model in the form of Stanton number $h/c_p\rho V$ against the dimensionless length l/b for various Mach number and Reynolds number conditions. All Stanton numbers shown are based on local conditions.

The transition point was located by using the variation of the Stanton number along the model in conjunction with the measured wall temperature. Figure 8 shows a typical variation of the wall temperature along the model for a specific time and Mach number.

Data for some of the Mach number and Reynolds number conditions were not presented because of low rates of change of the wall temperature with time (dT_w/dt) or low forcing functions ($T_{aw} - T_w$). Both of these conditions could cause large errors in the Stanton number.

Data obtained at the stagnation point will be discussed and correlated with existing theories later in this section.

Heat Transfer Along the Model

Figure 7(a) shows the data taken at $M = 2.00$ at 2.75 and 27.25 seconds at which times the free-stream Reynolds numbers per foot were 13.50×10^6 and 4.10×10^6, respectively. The data obtained at a Reynolds number per foot of 13.50×10^6 (2.75 seconds) appear to be laminar up to $l/b = 0.167$. The data taken at the following station ($l/b = 0.333$) show a considerable rise in Stanton number. This rise suggests transition from laminar to turbulent flow and occurs between a Reynolds number of 1.18×10^6 and 2.36×10^6, based on free-stream conditions and length from the stagnation point to the corresponding stations. The heating condition T_w/T_l is approximately 0.65 for this region of transition. Stanton numbers at stations rearward of $l/b = 0.333$ along the model show a gradual decrease, as might be expected for turbulent heat transfer. At a reduced Reynolds number per foot equal to 4.10×10^6 (27.25 seconds), the data appear to decrease rapidly as l/b increases;

this condition indicates laminar flow. However, at $l/b = 4.82$, a joint in the fuselage (designated herein as "nose joint") existed which apparently trips the boundary layer since all measurements rearward of this point are of turbulent magnitude. The calculated estimates for laminar flow are from the theories of Stine and Wanlass (ref. 4) and Van Driest (ref. 5). Both theories are in fair agreement with the data. For turbulent flow, the value of N_{St} calculated by using the Van Driest theory (ref. 6) for this condition (27.25 seconds) is about 20 percent higher than the data. It is interesting to note, however, that, if the theory were not modified as suggested in reference 14 and the straight Reynolds analogy $\left(N_{St} = \frac{1}{2} c_f\right)$ were used, the theory would then be in better agreement with the data. This point is true for all other Mach numbers. The flat-plate theories of Van Driest are valid only for the cylinder and do not consider the pressure gradient along the surface of the hemisphere. The theories in all cases are based on length from the stagnation point and on local flow conditions for the times indicated in the figure. Similar agreement with turbulent theory was obtained for flight conditions at 2.75 seconds but was not shown in figure 7(a).

For a Mach number of 2.50 (fig. 7(b)), the Stanton numbers are presented for Reynolds numbers per foot equal to 16.60×10^6, 13.00×10^6, and 7.55×10^6 corresponding to flight times of 3.20, 5.45, and 16.70 seconds, respectively. For a free-stream Reynolds number per foot of 16.60×10^6, transition occurs again between $l/b = 0.167$ and $l/b = 0.333$ for a value of $R_{\infty,T}$ between 1.44×10^6 and 2.90×10^6. The heating condition was approximately 0.60. For a slightly reduced Reynolds number per foot equal to 13.00×10^6, transition occurs back on the cylinder between stations $l/b = 3.23$ and $l/b = 3.86$. This Reynolds number of transition is between 21.80×10^6 and 26.20×10^6, which is a large increase in $R_{\infty,T}$ from the previous case at this Mach number. The heating condition was approximately 1.3. For the third condition where the Reynolds number per foot is equal to 7.55×10^6, laminar flow existed up to the nose joint at $l/b = 4.82$. This nose joint appears to have again tripped the boundary layer. The laminar theories are in good agreement whereas the turbulent theory is again higher than the data as for the $M = 2.00$ case. The theories are presented for the flight conditions at 16.70 seconds and it was assumed that the turbulent boundary layer was in existence from the stagnation point.

Data are presented for four flight times along the trajectory when $M = 2.80$ occurs. (See fig. 7(c).) These times correspond to 3.45, 4.62, 17.05, and 21.45 seconds for which the free-stream Reynolds numbers per foot are 17.80×10^6, 17.0×10^6, 8.30×10^6, and 6.90×10^6, respectively.

[redacted]

For $t = 3.45$ seconds or for the free-stream Reynolds number per foot equal to 17.80×10^6, transition occurs again between $l/b = 0.167$ and $l/b = 0.333$ for a value of $R_{\infty,T}$ between 1.55×10^6 and 3.10×10^6. For about the same Reynolds number per foot (17.00×10^6) at $t = 4.62$ seconds, transition started at $l/b = 0.333$ which corresponds to $R_{\infty,T} = 3.0 \times 10^6$. It is interesting to note that the heating condition for both conditions was approximately 1.0. For the two lower Reynolds number conditions, laminar heat transfer prevailed up to the nose joint at $l/b = 4.82$, and the data are in agreement with the laminar theories. Turbulent heat-transfer data are again lower than theory.

For a Mach number of 3.05 and for the low free-stream Reynolds numbers per foot equal to 8.84×10^6 and 7.83×10^6 obtained at 17.30 and 20.40 seconds, respectively, laminar flow existed up to the nose joint. However, for $t = 3.80$ seconds (Reynolds number per foot equal to 18.90×10^6), transition occurred closer to the stagnation point between stations $l/b = 0.083$ and $l/b = 0.167$ or for $R_{\infty,T} = 0.824 \times 10^6$ for the station $l/b = 0.083$. The theory for laminar flow showed good agreement with the measurements whereas the turbulent heat-transfer data were in similar agreement with turbulent theory as for the preceding Mach number cases.

Data are presented at a Mach number of 3.40 for Reynolds numbers per foot equal to 9.80×10^6 and 9.10×10^6 which correspond to flight times of 17.70 and 19.45 seconds. (See fig. 7(e).) Here again the data appear to be laminar up to the nose joint when the Reynolds number per foot is 9.80×10^6; whereas, for the other conditions at $t = 19.45$ seconds when the Reynolds number per foot is 9.10×10^6, transition appears between $l/b = 1.48$ and $l/b = 1.96$ which gives $R_{\infty,T} = 7.05 \times 10^6$ for $l/b = 1.48$. However, the data do not reach full turbulent level until $l/b = 3.86$. The agreement with theory is again as good as for the previous Mach numbers.

In figure 7(f) is shown the data taken at $M = 3.60$ for Reynolds numbers per foot equal to 10.40×10^6 and 9.60×10^6 which occur at times 17.90 and 19.00 seconds, respectively. For a Reynolds number per foot of 10.40×10^6, the data appeared to be laminar to $l/b = 1.96$ $\left(R_{\infty,T} = 10.7 \times 10^6\right)$; however, some rise above the laminar theory is noted and this rise might suggest that transition had started. This region of transition occurs for a constant T_w/T_l of approximately 0.95. For the other test condition (19.00 seconds), the transition region begins close

to the hemisphere-cylinder junction $l/b = 1.48$ $\left(R_{\infty,T} = 7.45 \times 10^6\right)$ and extends to $l/b = 3.86$. This rise occurs for a $T_w/T_l = 1.10$ at $l/b = 1.48$ to $T_w/T_l = 0.95$ at $l/b = 3.86$. The laminar theory (ref. 4) is in agreement with the data whereas the turbulent theory is higher than the measurements.

Only one test condition appears for a Mach number 3.88 (fig. 7(g)), this being the highest Mach number of the test. The Reynolds number per foot is 10.80×10^6. Figure 7(g) again shows the agreement with the laminar theory and transition is shown by the rise in the Stanton number at $l/b = 1.48$ which occurs for $T_w/T_l = 0.95$ and $R_{\infty,T} = 8.22 \times 10^6$. The agreement with the turbulent theory is again considerably lower.

From preceding test conditions, it appears that laminar theory gives a good prediction for the heat-transfer coefficient whereas the turbulent theory overestimates the heat-transfer coefficient. This discrepancy in the turbulent theory has also been noticed in other heat-transfer investigations for blunt-nosed bodies. (See ref. 1.)

Stagnation-Point Heat Transfer

In figure 9 is presented the measured stagnation-point heat transfer expressed as $\frac{N_{Nu}}{\sqrt{\rho\beta D^2/\mu}}$ as a function of Mach number, where the air properties in the heat-transfer parameter are based on the stagnation-point conditions and the Nusselt number is based on the diameter of the cylinder. Values of β are given as functions of Mach number by Korobkin (ref. 15). The data are compared with the theory of Sibulkin (ref. 3). The data appear to scatter about the theory and are in fair agreement. However, some of the data points fall considerably below the theoretical predictions. Similar results from flight test and the theory of reference 16 have suggested lower heat-transfer coefficients than those of reference 3.

Boundary-Layer Transition

Transition was pointed out in the discussion of heat-transfer measurements. At attempt to correlate the Reynolds number of transition for the hemispherical section was made by taking the various locations on the body for which the heat-transfer coefficient shows a sudden increase and expressing this rise at the start of transition.

The Reynolds numbers of transition were plotted as functions of the free-stream Reynolds number based on the surface length from the

stagnation point to the junction of the hemisphere-cylinder ($l/b = 1$) in figure 10. The solid symbols signify that transition occurred on the hemisphere. The figure indicates that, if the Reynolds number to the junction is greater than approximately 6×10^6, transition appeared in the subsonic flow region and the Reynolds number of transition is low $\left(0.8 \times 10^6 \text{ to } 3.0 \times 10^6\right)$; however, when the Reynolds number is less than 6×10^6, transition occurred in the supersonic flow region and the Reynolds number of transition may vary from 7.0×10^6 to 24.7×10^6. The transition points on the hemisphere were in accord with the transition Reynolds number experienced on a 4-inch-diameter hemisphere tested in a free jet (ref. 2) and with other flight tests of a hemisphere-cone model partly reported in reference 1. For convenience in comparing transition with other tests, the Reynolds number of transition based on computed momentum thickness R_θ is given in figure 10 for points of transition on the hemisphere and one value is given for transition at the nose joint ($l/b = 4.82$). The values of R_θ were computed by the method of reference 17.

SUMMARY OF RESULTS

Measurements of aerodynamic heat transfer have been made at 23 stations along the body of a hemisphere-cylinder rocket-propelled model up to a Mach number of 3.88. Data are presented for a range of free-stream Reynolds number, based on the diameter of the model, between 2.69×10^6 and 11.70×10^6. Laminar, transitional, and turbulent heat-transfer coefficients were measured and the following results noted:

1. The laminar data agreed with theory for a hemisphere-cylinder body. The turbulent data, on the cylinder, were consistently lower than predicted by the turbulent heat-transfer theory for a flat plate.

2. Measurements made at the stagnation point were lower than predicted by theory but are consistent with other similar investigations.

3. When the Reynolds number to the junction of the hemisphere-cylinder was greater than approximately 6×10^6, the transitional Reynolds number varied from 0.8×10^6 to 3.0×10^6; however, when the Reynolds number to the junction was less than 6×10^6, the transition Reynolds number varied from 7.0×10^6 to 24.7×10^6.

Langley Aeronautical Laboratory,
National Advisory Committee for Aeronautics,
Langley Field, Va., March 29, 1957.

REFERENCES

1. Chauvin, Leo T.: Aerodynamic Heating of Aircraft Components. NACA RM L55L19b, 1956.

2. Chauvin, Leo T., and Maloney, Joseph P.: Experimental Convective Heat Transfer to a 4-Inch and 6-Inch Hemisphere at Mach Numbers From 1.62 to 3.04. NACA RM L53L08a, 1954.

3. Sibulkin, M.: Heat Transfer Near the Forward Stagnation Point of a Body of Revolution. Jour. Aero. Sci., vol. 19, no. 8, Aug. 1952, pp. 570-571.

4. Stine, Howard A., and Wanlass, Kent: Theoretical and Experimental Investigation of Aerodynamic-Heating and Isothermal Heat-Transfer Parameters on a Hemispherical Nose With Laminar Boundary Layer at Supersonic Mach Numbers. NACA TN 3344, 1954.

5. Van Driest, E. R.: Investigation of Laminar Boundary Layer in Compressible Fluids Using the Crocco Method. NACA TN 2597, 1952.

6. Van Driest, E. R.: Turbulent Boundary Layer in Compressible Fluids. Jour. Aero. Sci., vol. 18, no. 3, Mar. 1951, pp. 145-160, 216.

7. Rumsey, Charles B., and Lee, Dorothy B.: Measurements of Aerodynamic Heat Transfer and Boundary-Layer Transition on a 10° Cone in Free Flight at Supersonic Mach Numbers up to 5.9. NACA RM L56B07, 1956.

8. Crawford, Davis H., and McCauly, William D.: Investigation of the Laminar Aerodynamic Heat-Transfer Characteristics of a Hemisphere-Cylinder in the Langley 11-Inch Hypersonic Tunnel at a Mach Number of 6.8. NACA TN 3706, 1956.

9. Chauvin, Leo T.: Pressure Distribution and Pressure Drag for a Hemispherical Nose at Mach Numbers 2.05, 2.54, and 3.04. NACA RM L52K06, 1952.

10. Oliver, Robert E.: An Experimental Investigation of Flow Over Simple Blunt Bodies at a Nominal Mach of 5.8. GALCIT Memo. No. 26. (Contract No. DA-04-495-Ord-19), June 1, 1955.

11. Anon. (Compiled by F. C. Morey): The NBS-NACA Tables of Thermal Properties of Gases. Nat. Bur. Standards, 1950.

12. Ginnings, Defoe C., and Thomas, Eugenia: The Electrical Resistance and Total Radiant Emittance of Inconel in the Range 0° to 1000° C. NBS Rep. 4111 (NACA Contract S54-52), Nat. Bur. Standards, May 1955.

13. Kelly, K. K.: Contributions to the Data on Theoretical Metallurgy. II. High-Temperature Specific-Heat Equations for Inorganic Substances. Bulletin 371, Bur. Mines, 1934.

14. Rubesin, Morris W.: A Modified Reynolds Analogy for the Compressible Turbulent Boundary Layer on a Flat Plate. NACA TN 2917, 1953.

15. Korobkin, Irving: Laminar Heat Characteristics of a Hemisphere for the Mach Number Range 1.9 to 4.9. NAVORD Rep. 3841 (Aeroballistic Res. Rep. 257) U. S. Naval Ord. Lab. (White Oak, Md.), Oct. 10, 1954.

16. Probstein, Ronald F.: The Effect of Variable Fluid Properties on the Equilibrium Laminar Boundary Layer Surface Heat Transfer Rate At Hypersonic Flight Speeds. WADC TN 56-2 (Contract No. AF 33(616)-2798), Wright Air Dev. Center, U. S. Air Force, Dec. 1955.

17. Anon.: X-17 Re-entry Test Vehicle - R-1 Final Flight Report. Rep. No. MSD-1834 (Contract No. AF 04(645)-7), Lockheed Aircraft Corp., July 17, 1956.

TABLE I.- LOCATION OF THERMOCOUPLES

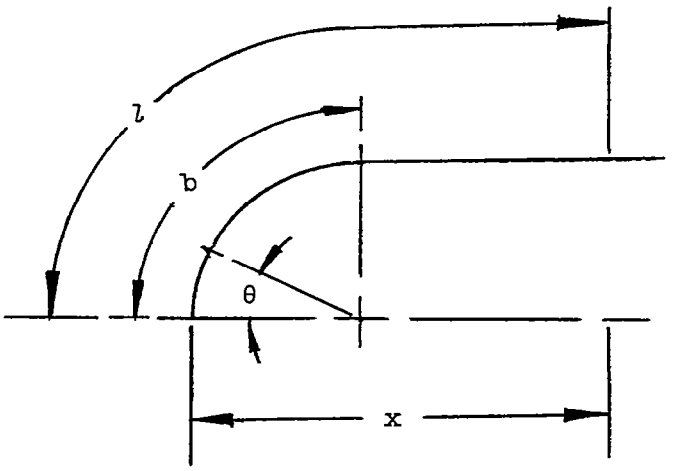

b = 6.28 in.

Thermocouple	θ, deg	x, in.	l, in.	l/b	Skin thickness, in.
1,2	0	0	0	0	0.040
3	7.5	.04	.524	.083	.040
4	15	.15	1.05	.167	.042
5	30	.54	2.09	.333	.042
6	60	2.00	4.19	.666	.032
7	90	4.00	6.28	1.000	.025
8	90	7.00	9.28	1.48	.034
9	90	10.00	12.28	1.96	.034
10	90	14.00	16.28	2.59	.034
11	90	18.00	20.28	3.23	.034
12	90	22.00	24.28	3.86	.034
13	90	37.25	39.53	6.30	.092
14	90	44.25	46.53	7.25	.092
15	90	51.25	53.53	8.54	.092
16	90	58.25	60.53	9.65	.092
17	90	65.25	67.53	10.78	.092
18	90	72.25	74.53	11.89	.092
19	90	82.25	84.53	13.64	.092
20	90	91.25	93.53	14.80	.092
21	90	100.25	102.53	16.32	.092
22	90	109.25	111.53	17.75	.092
23	90	118.25	120.53	19.18	.092

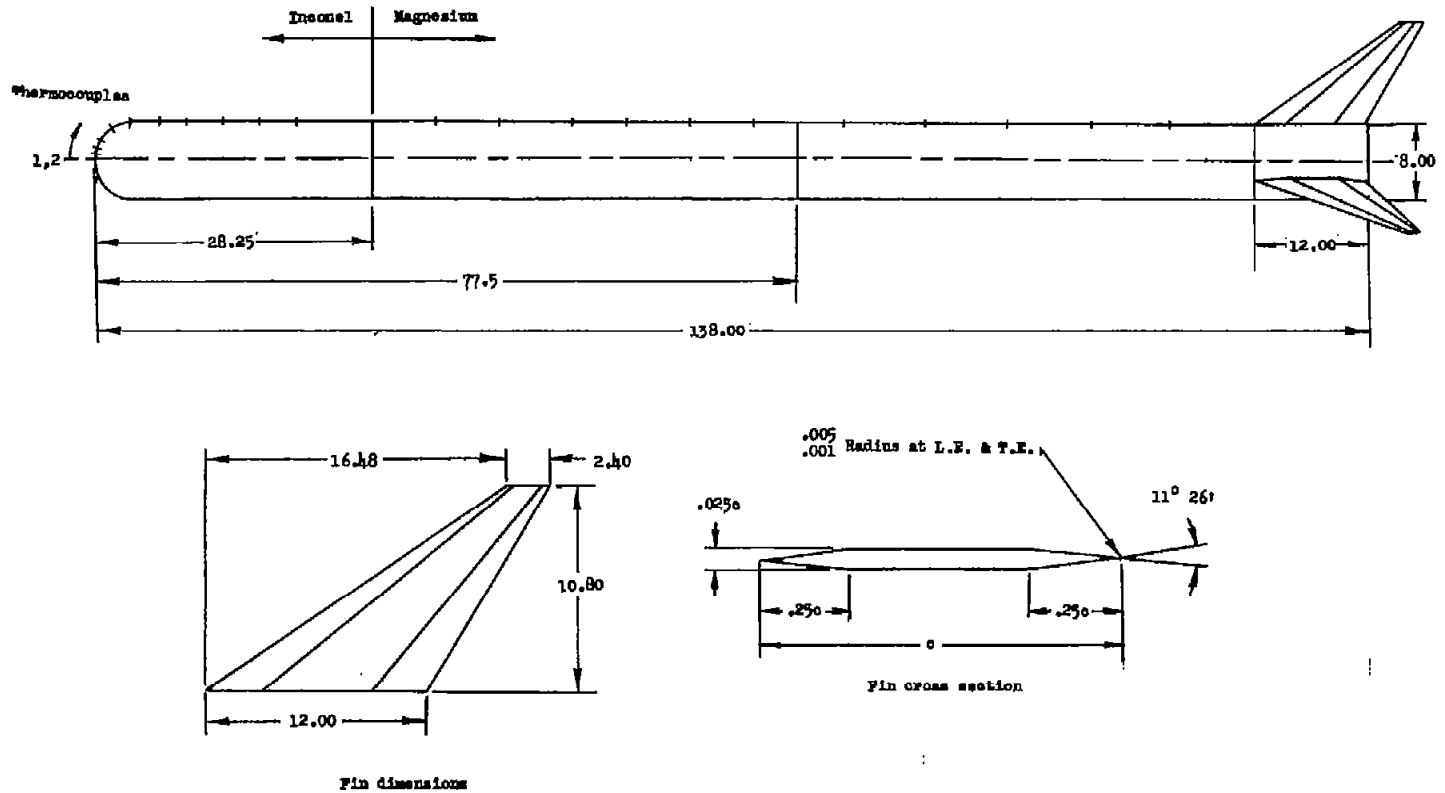

Figure 1.- General configuration of model.

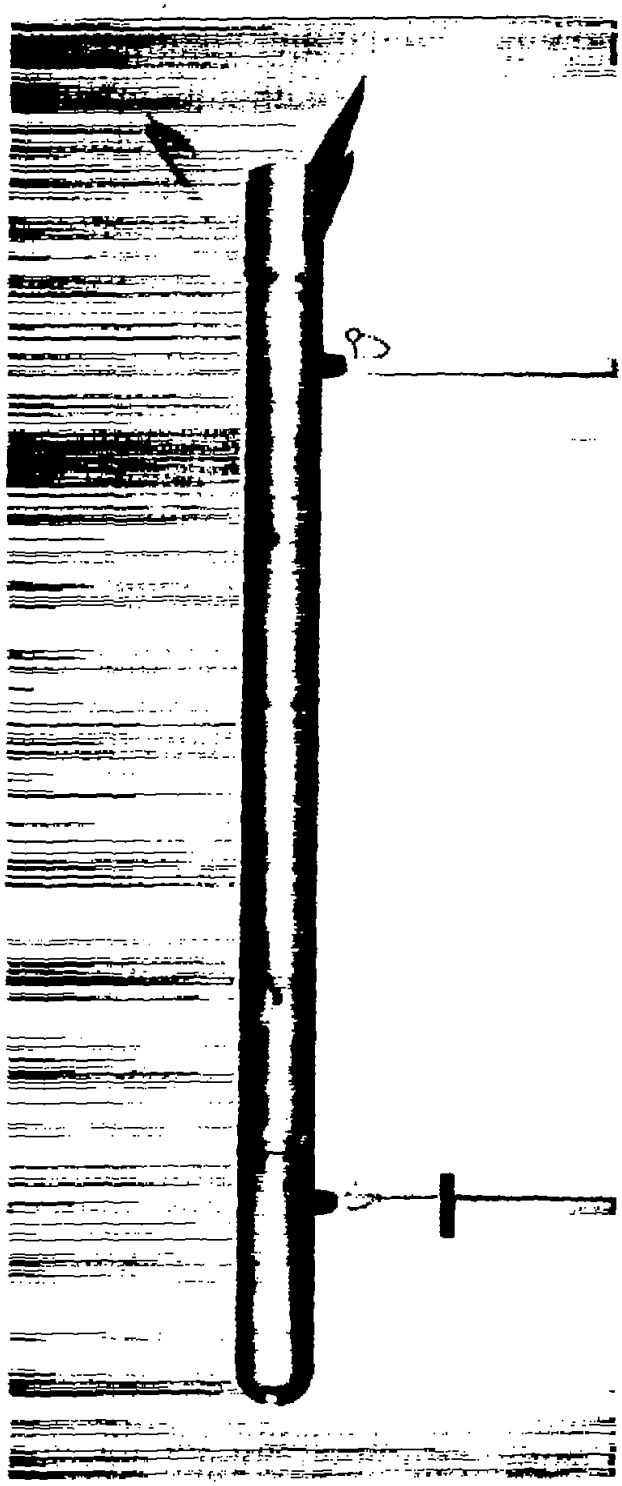

L-90407.1

Figure 2.- Photograph of model.

Figure 3.- Photograph of model and booster in launching position. L-91142

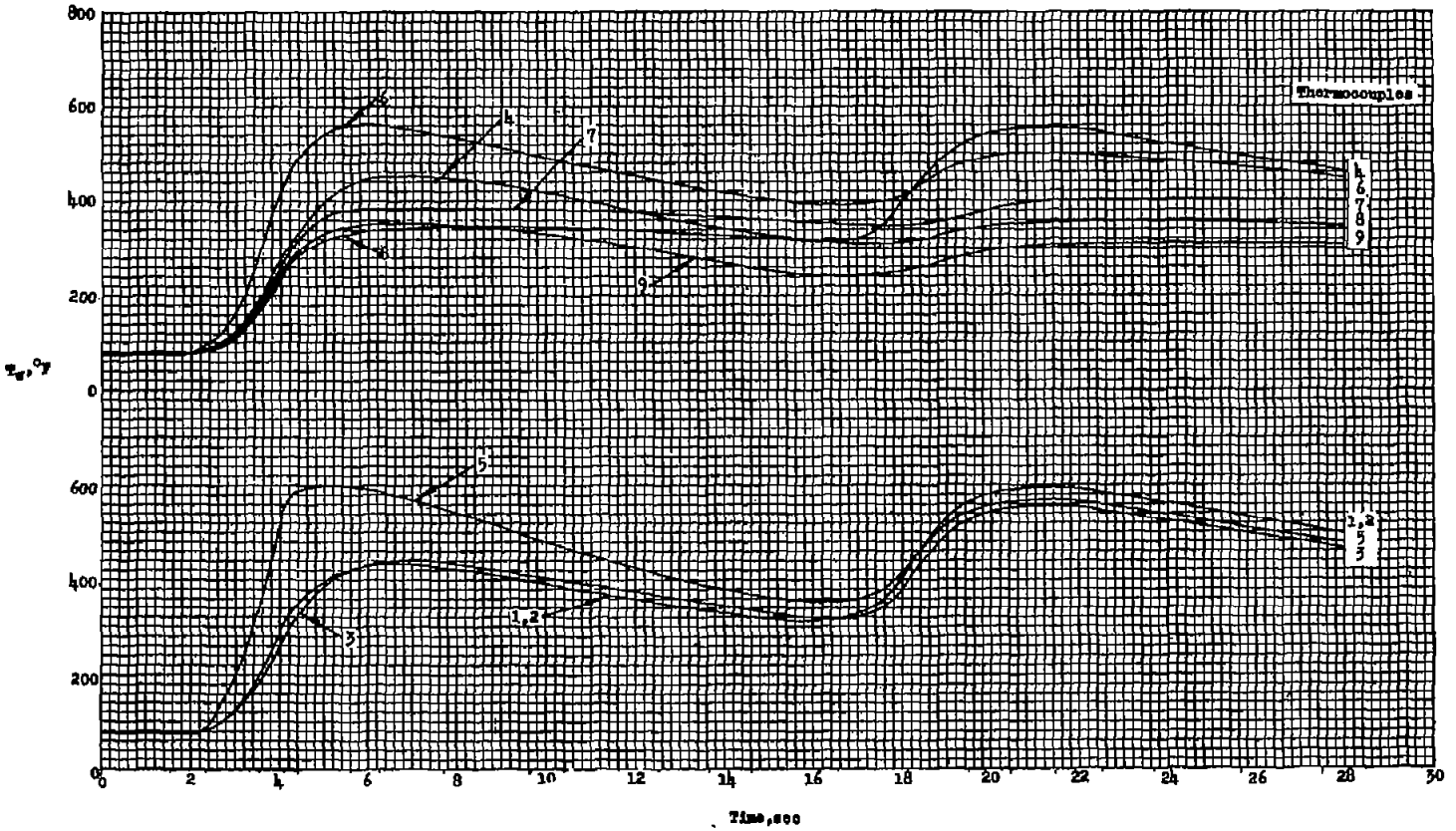

(a) Thermocouples 1 to 9.

Figure 4.- Wall-temperature time histories at several stations.

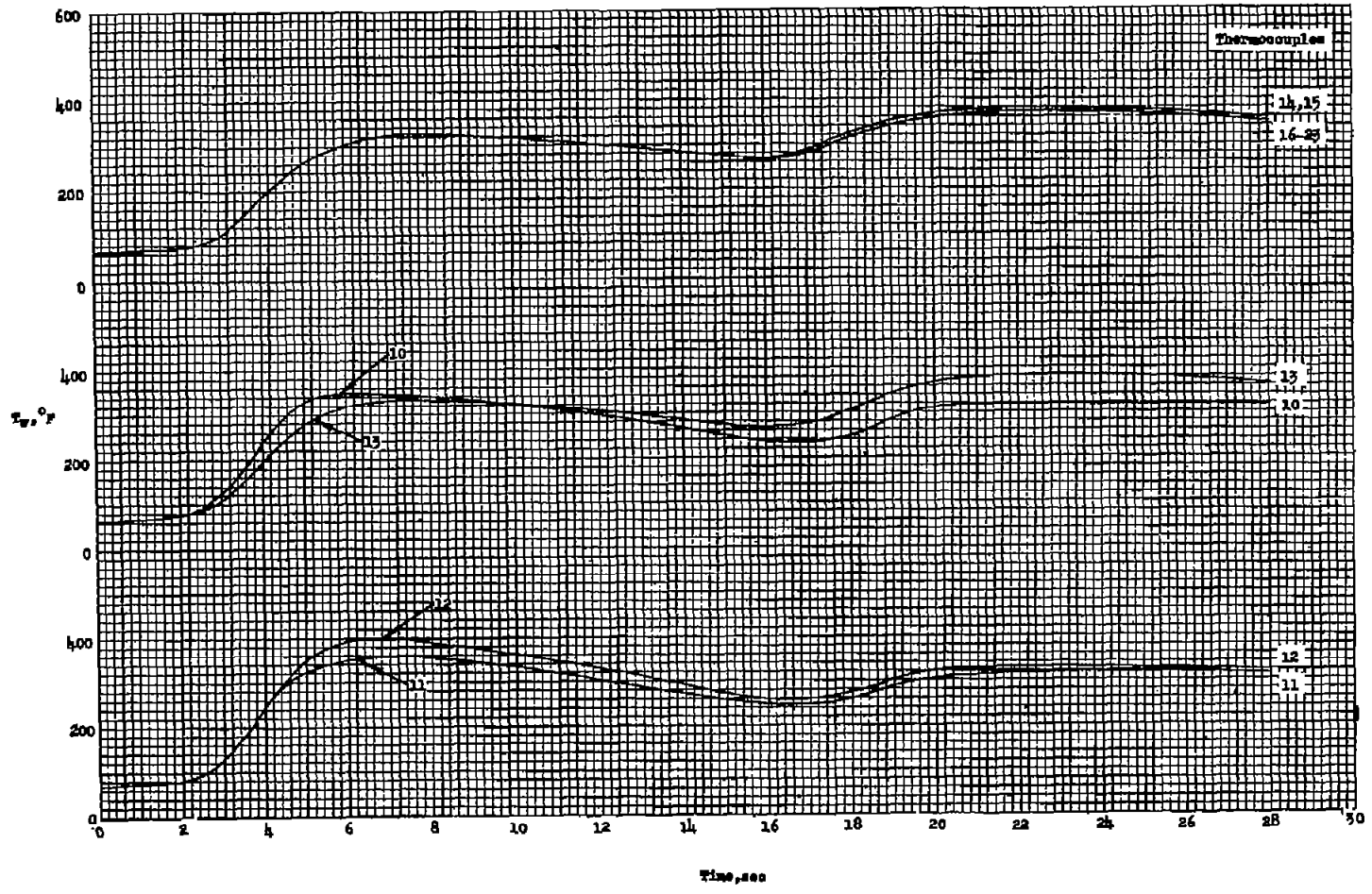

(b) Thermocouples 10 to 23.

Figure 4.- Concluded.

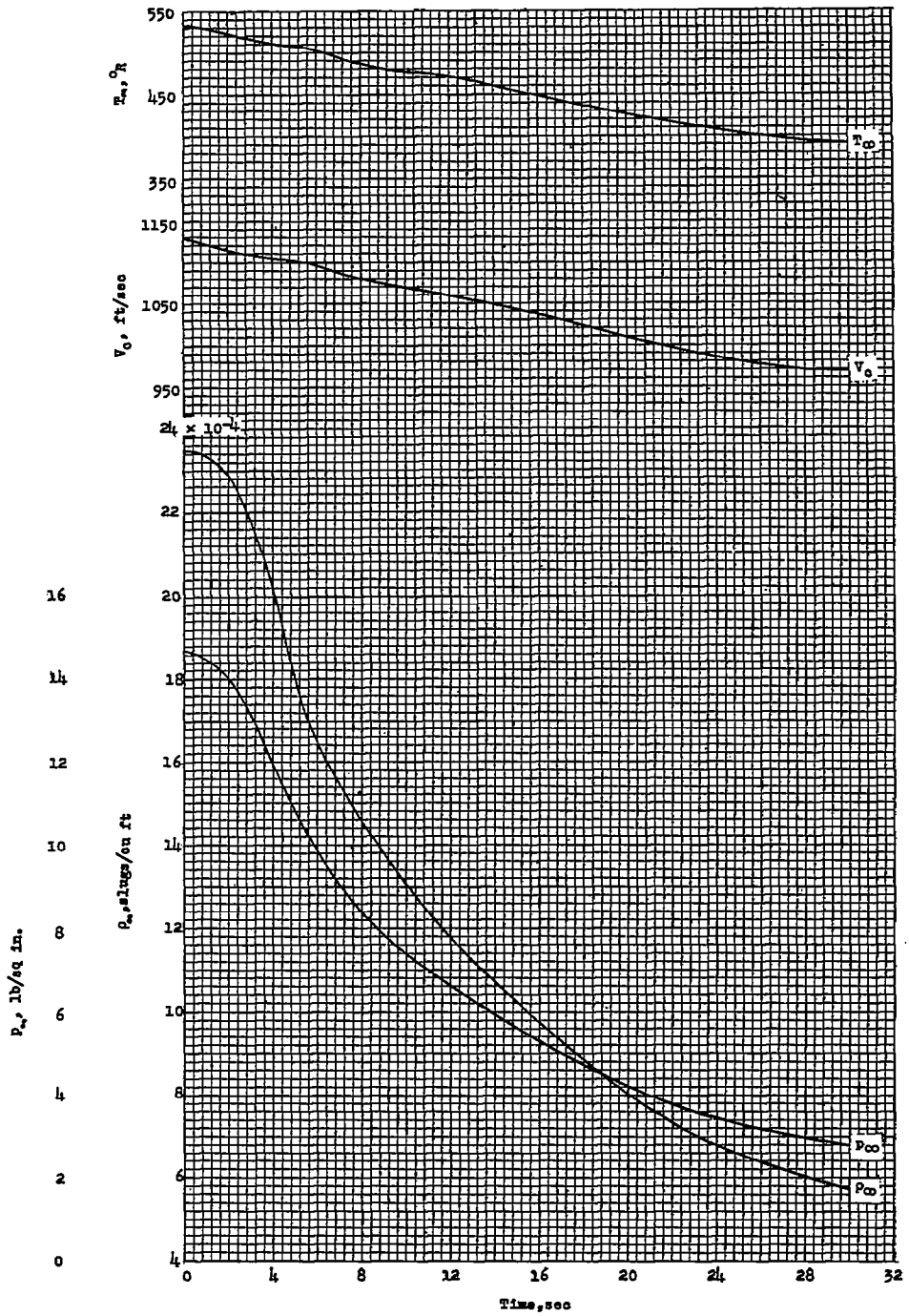

Figure 5.- Free-stream flight conditions.

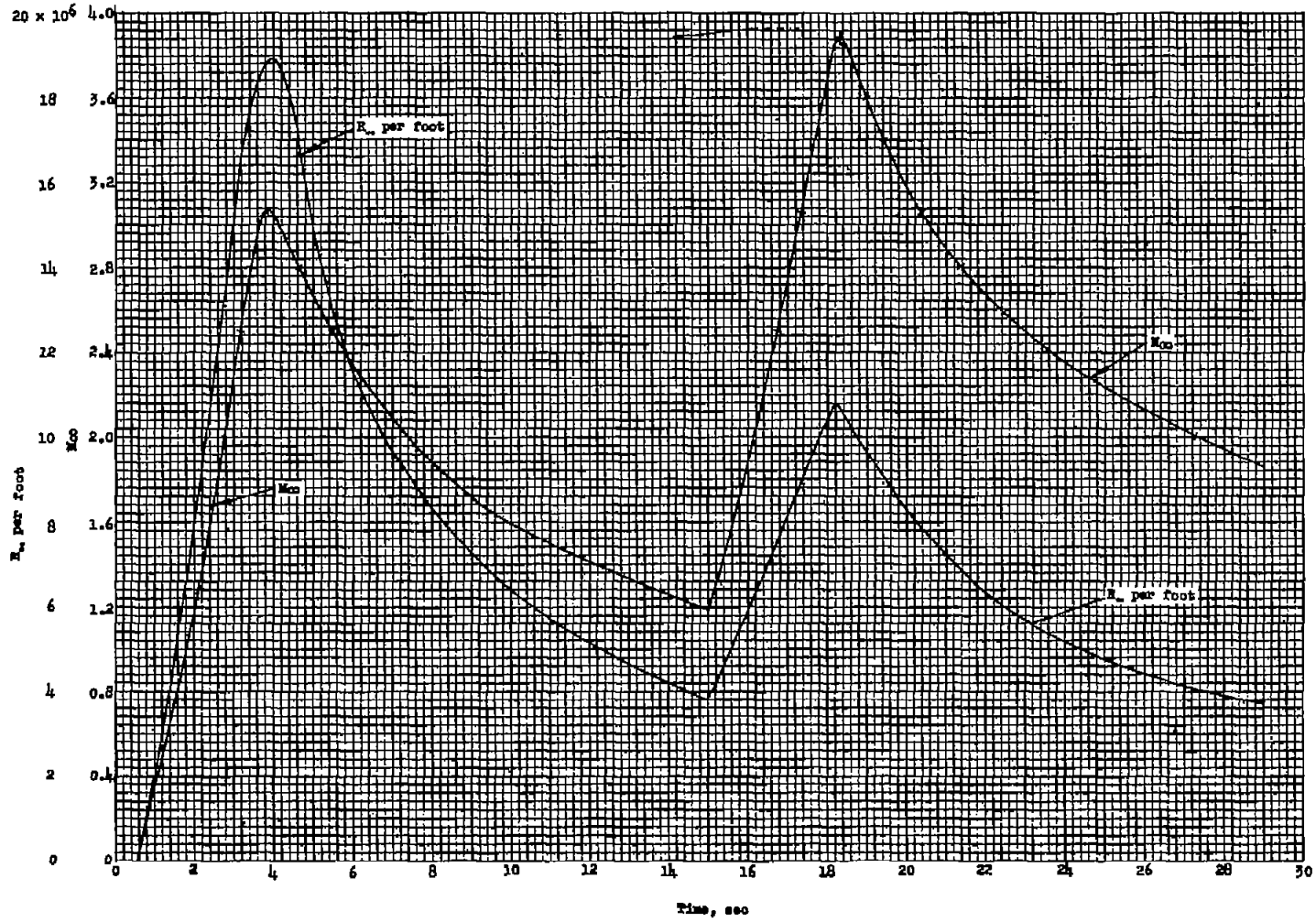

Figure 6.- Time histories of free-stream Mach number and Reynolds number.

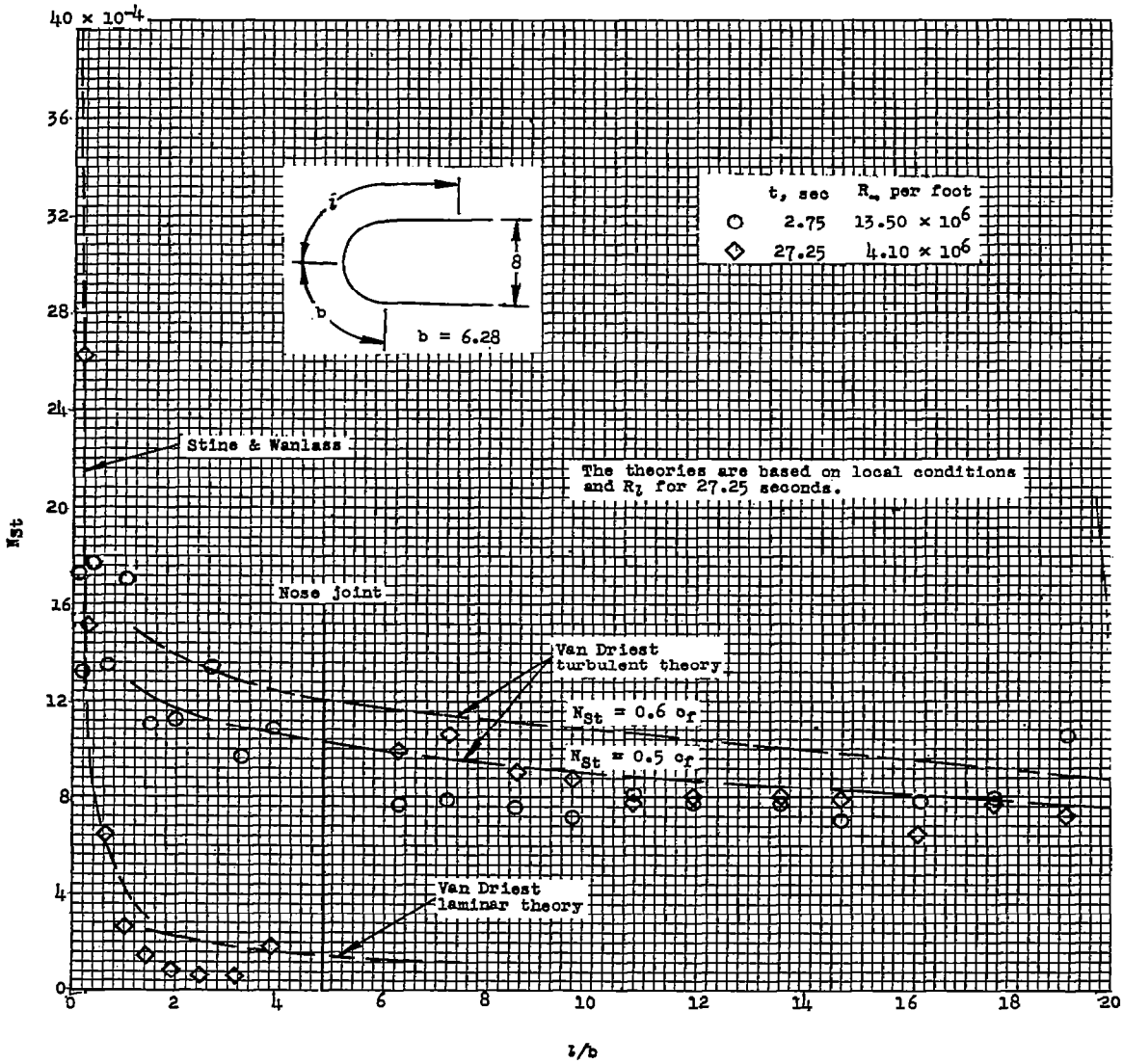

(a) $M_\infty = 2.00$.

Figure 7.- Stanton numbers along the model for a given M_∞ and for several R_∞ conditions.

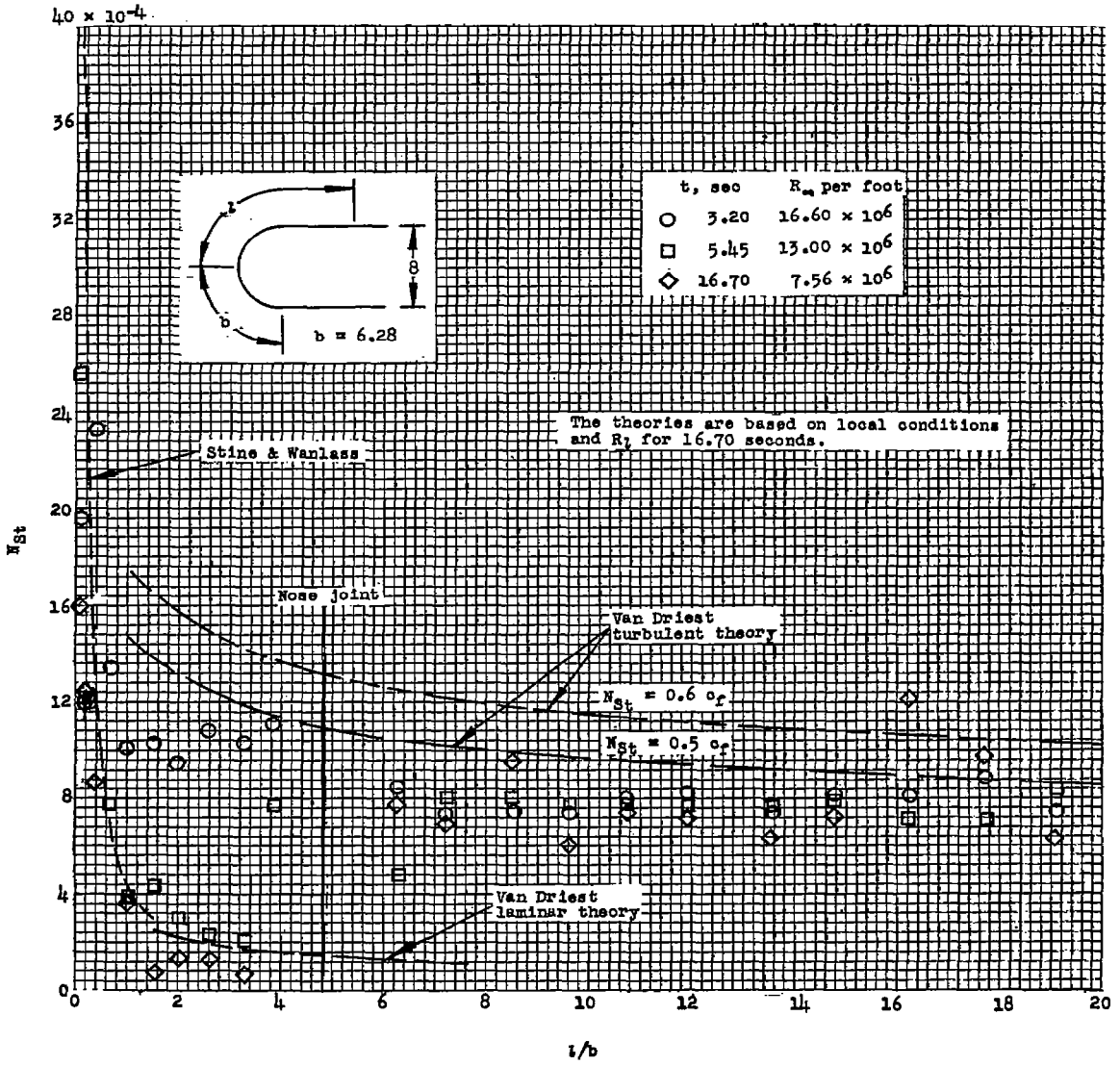

(b) $M_\infty = 2.50$.

Figure 7.- Continued.

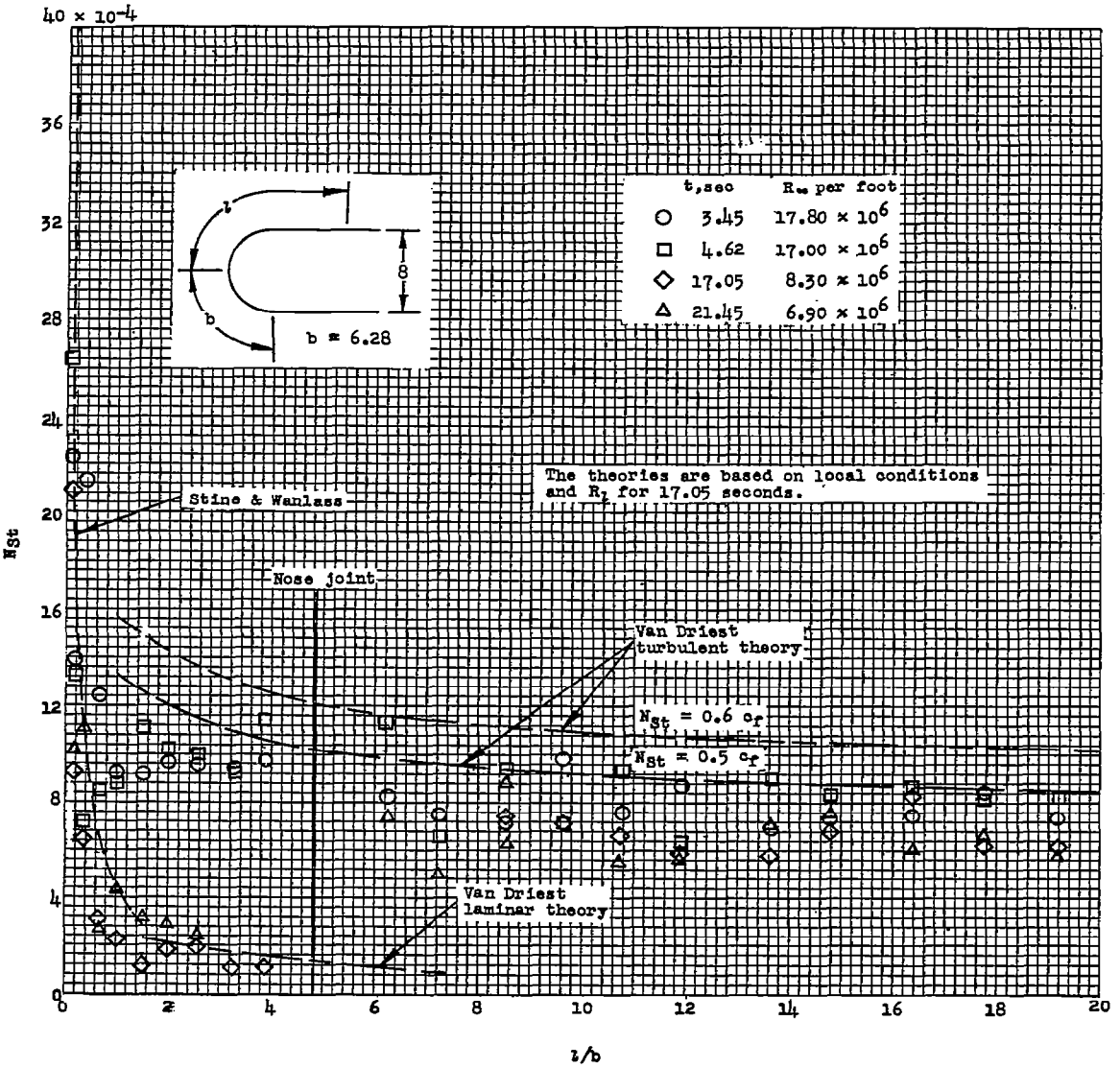

(c) $M_\infty = 2.80$.

Figure 7.- Continued.

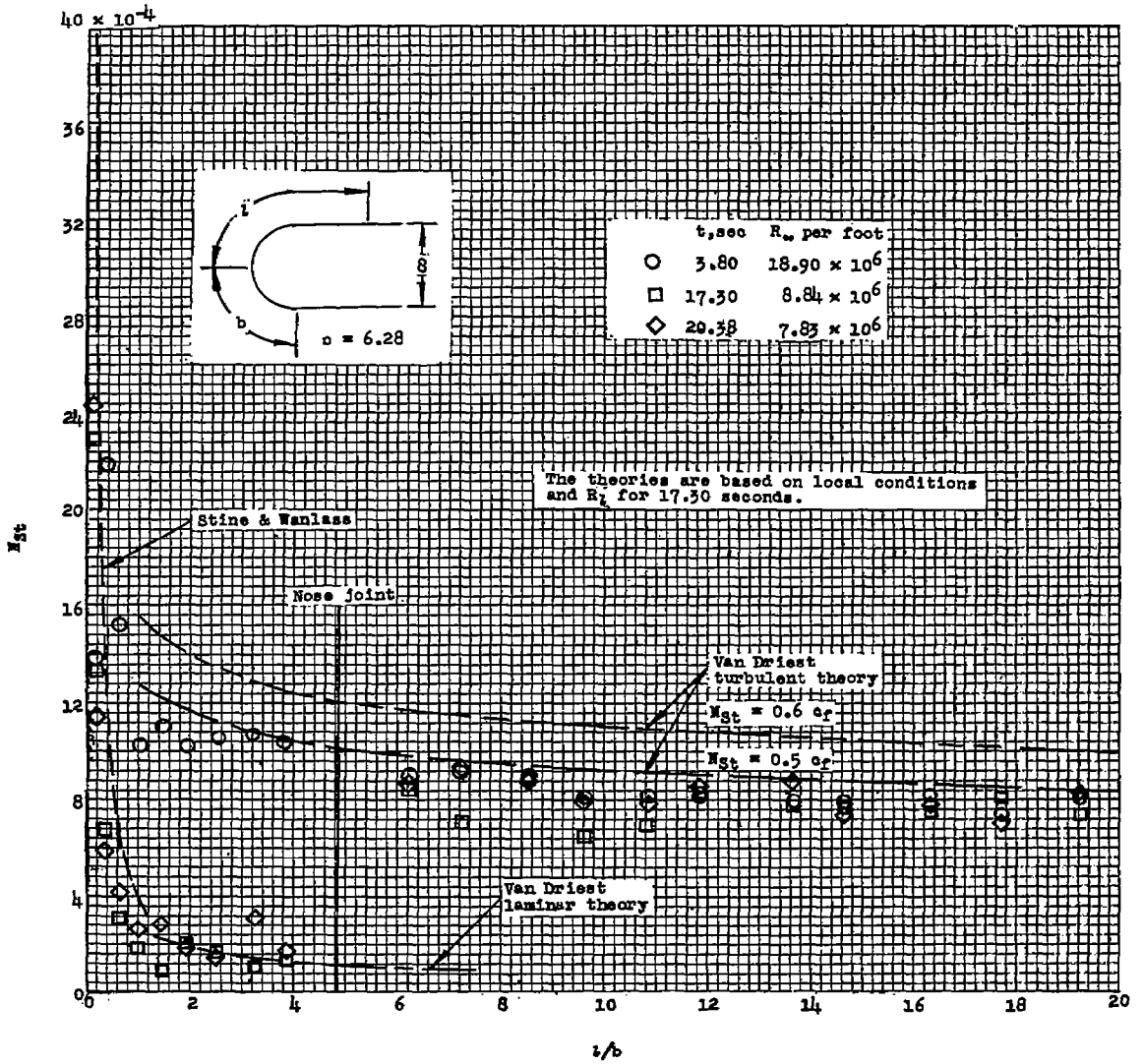

(d) $M_\infty = 3.05$.

Figure 7.- Continued.

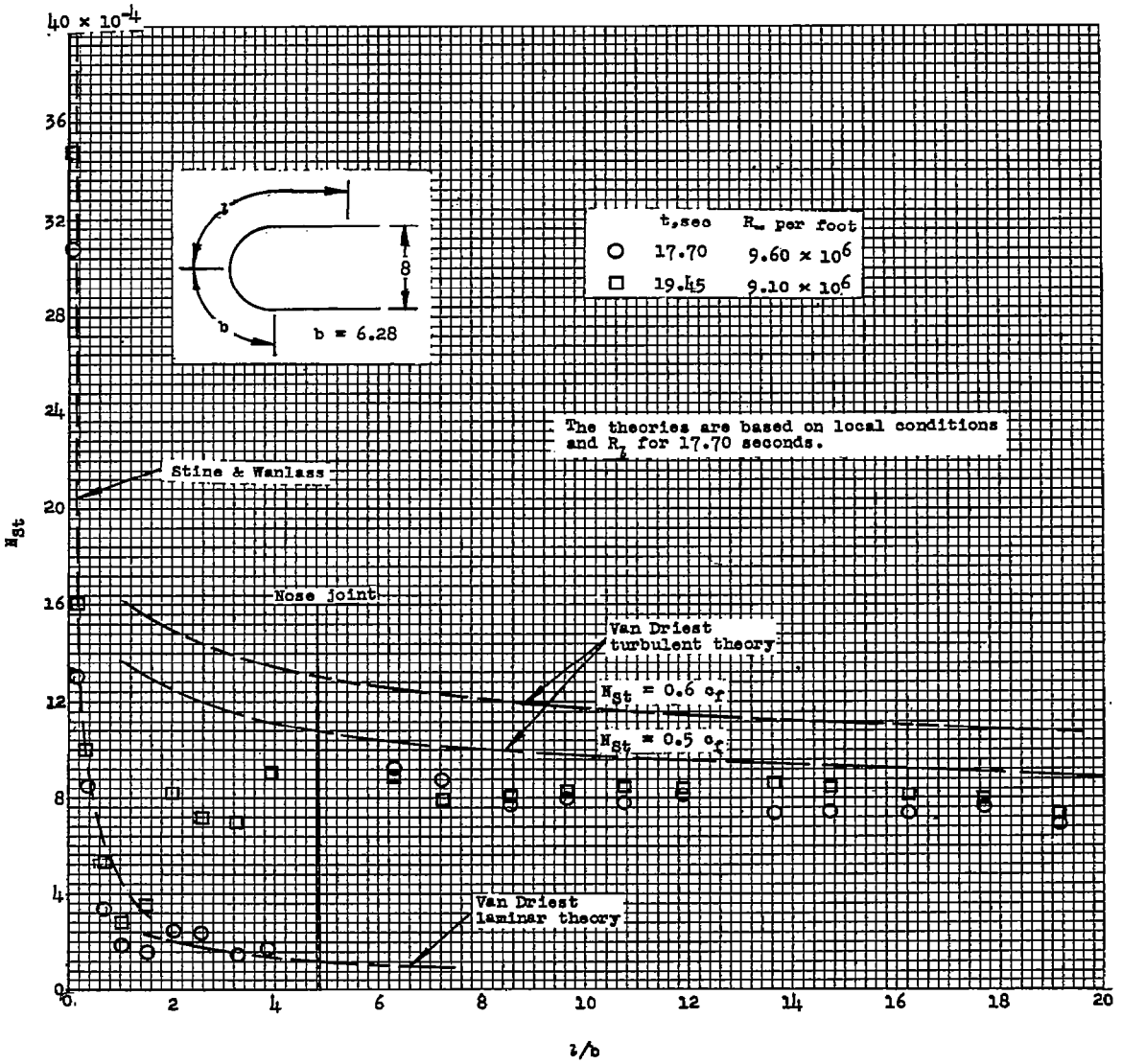

(e) $M_\infty = 3.40$.

Figure 7.- Continued.

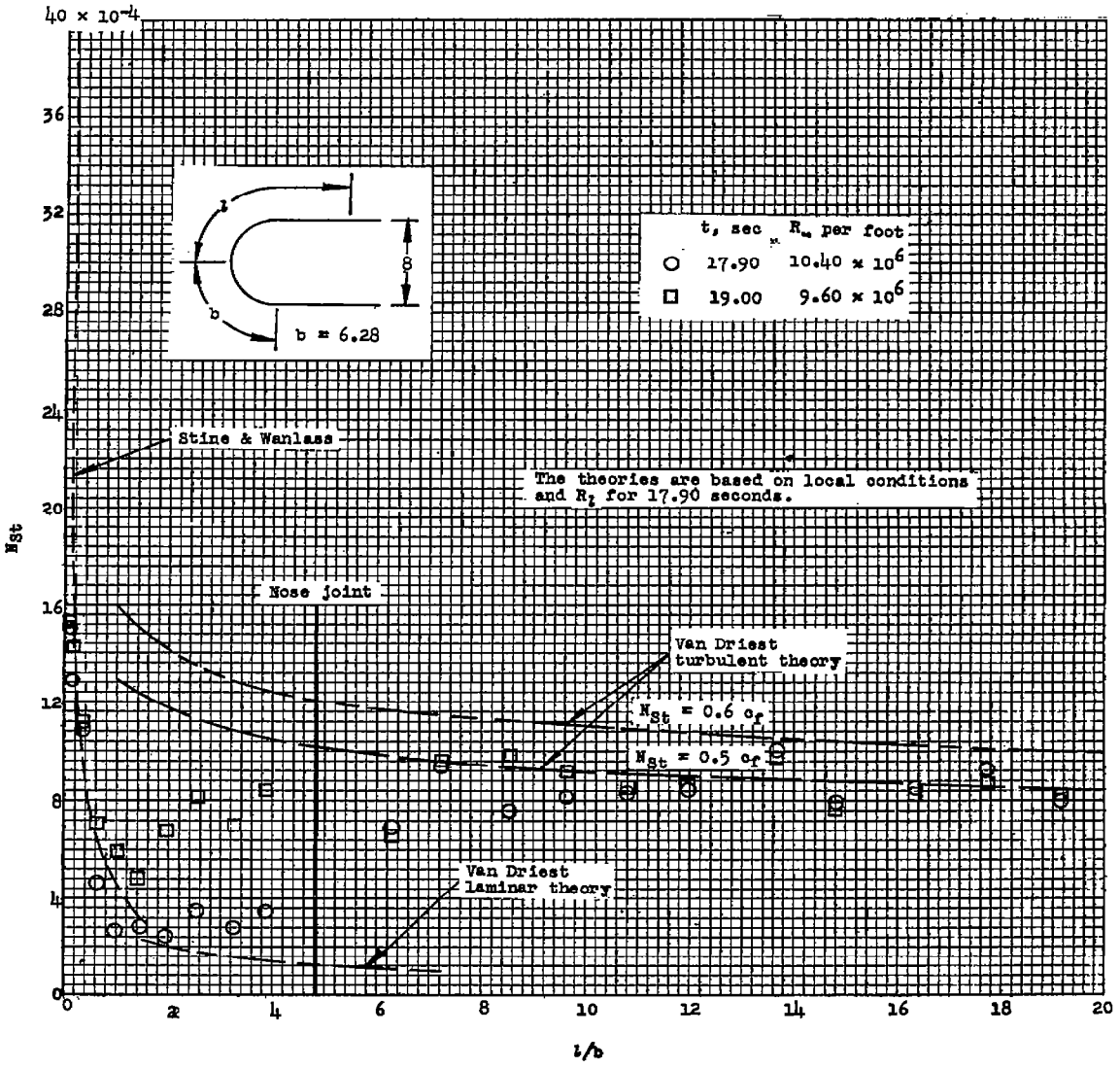

(f) $M_\infty = 3.60$.

Figure 7.- Continued.

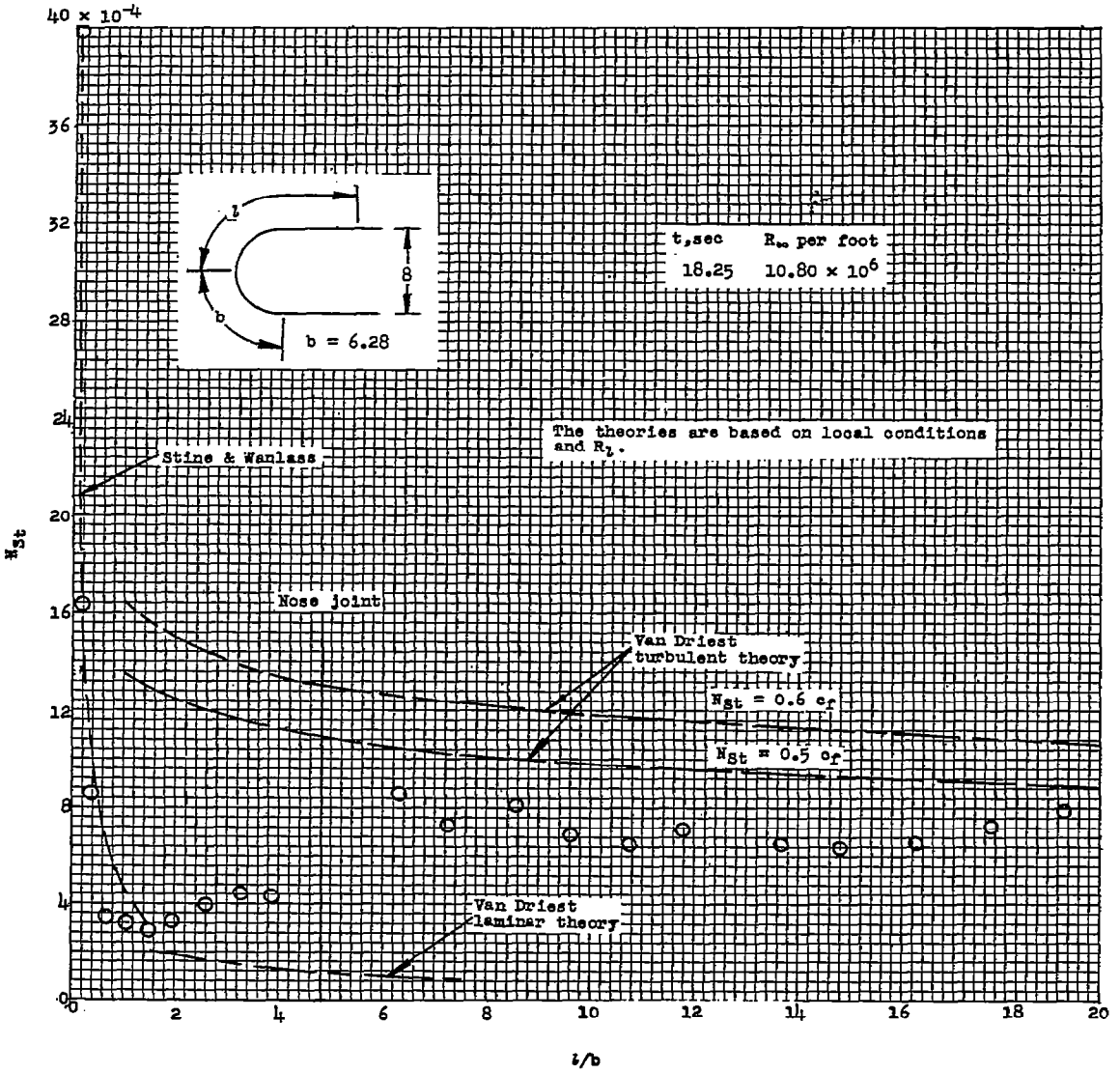

(g) $M_\infty = 3.88$.

Figure 7.- Concluded.

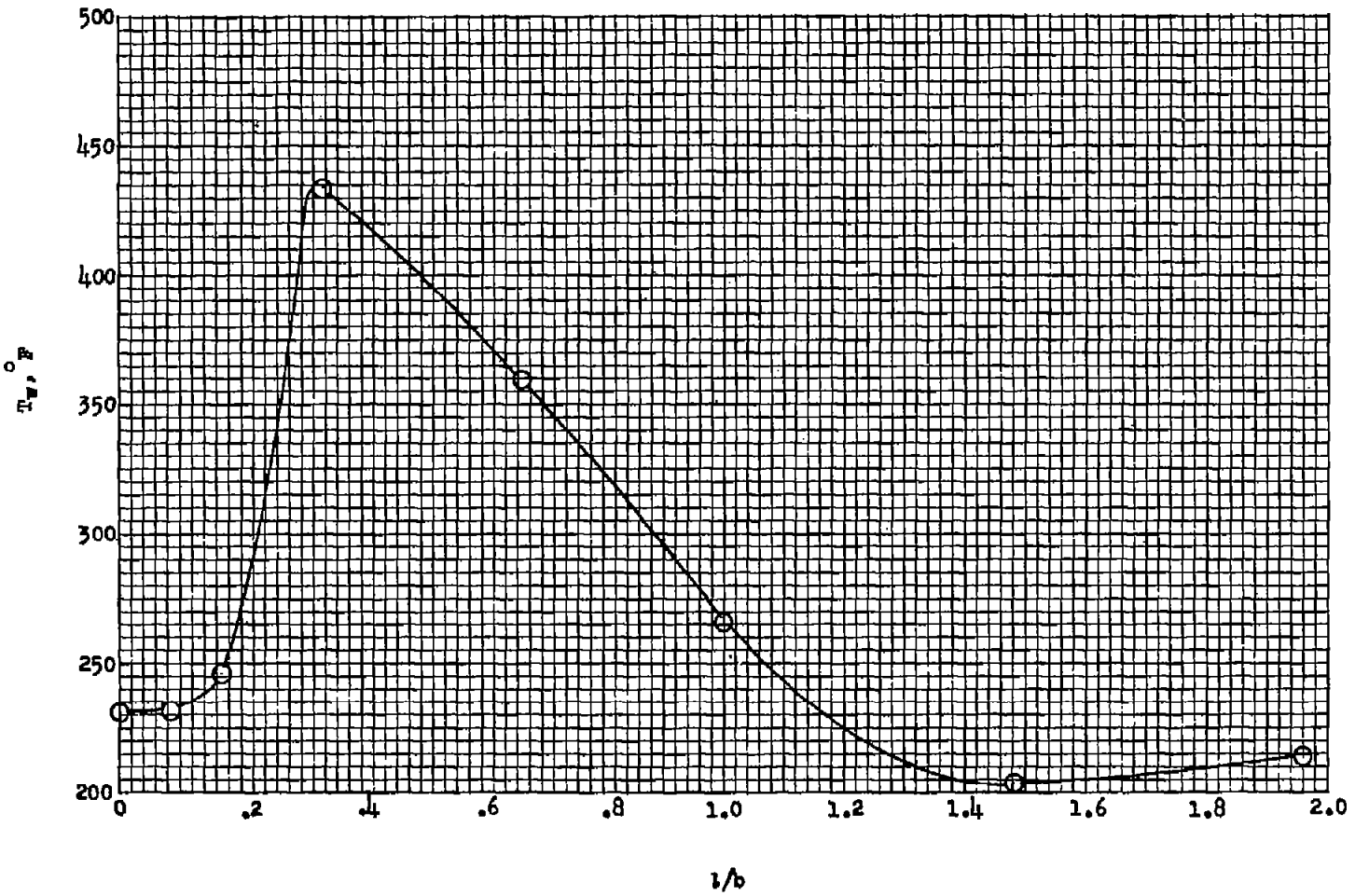

Figure 8.- Typical wall-temperature distribution along the model. $M_\infty = 3.05$; $t = 3.80$ seconds.

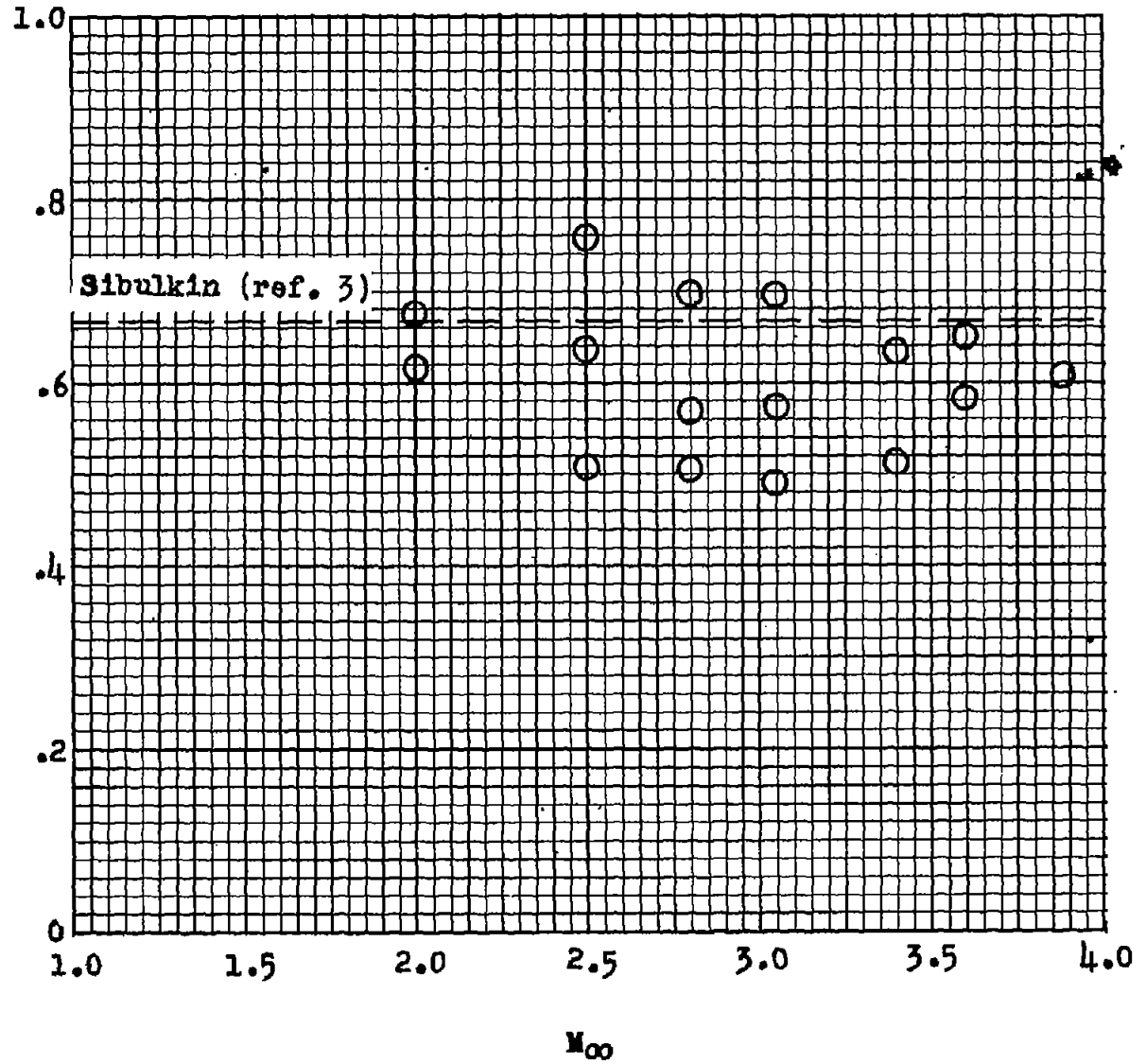

Figure 9.- Variation of stagnation-point heat-transfer parameter with Mach number.

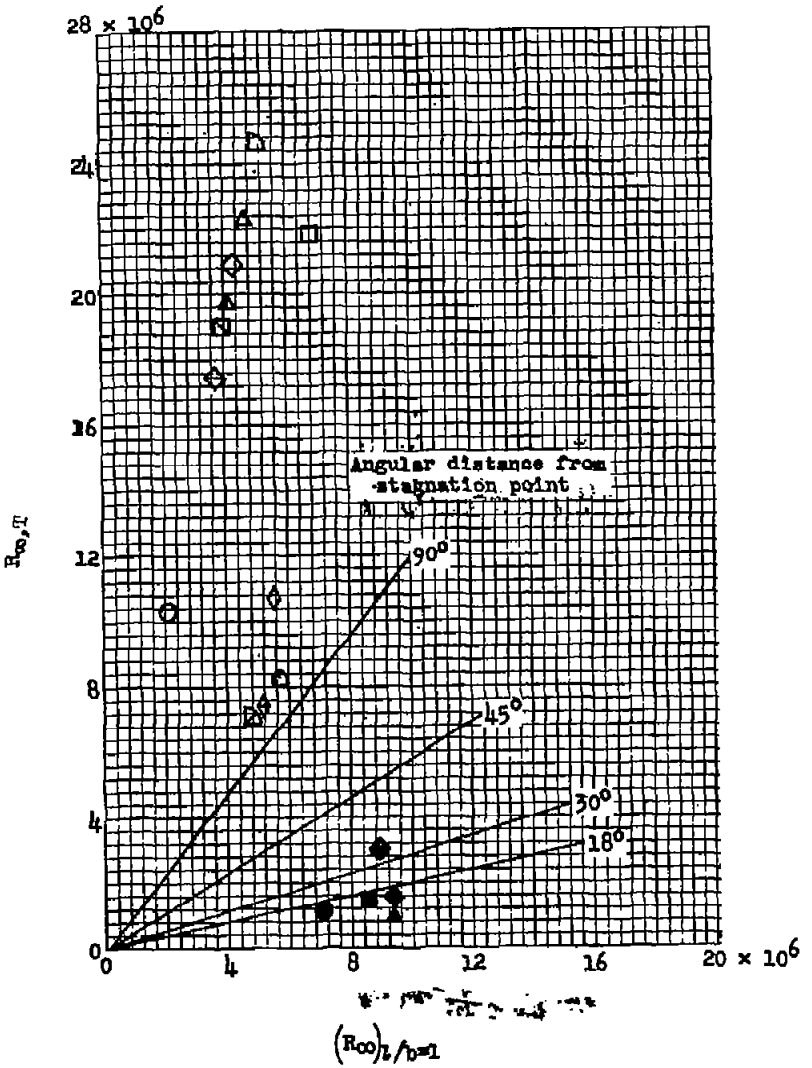

	M	R_∞ per foot	R_θ
●	2.00	13.50 × 10^6	268
○	2.00	4.10 × 10^6	
■	2.50	16.60 × 10^6	292
□	2.50	13.00 × 10^6	
⊠	2.50	7.55 × 10^6	
◆	2.80	17.80 × 10^6	294
◆	2.80	17.00 × 10^6	574
◇	2.80	8.30 × 10^6	
◈	2.80	6.90 × 10^6	
▲	3.05	18.90 × 10^6	159
△	3.05	8.84 × 10^6	
▲	3.05	7.83 × 10^6	
▷	3.40	9.80 × 10^6	1,900
▷	3.40	9.10 × 10^6	
◇	3.60	10.30 × 10^6	
◈	3.60	7.45 × 10^6	
⌂	3.88	10.80 × 10^6	

Solid symbols signify transition on the hemisphere

Figure 10.- Reynolds number of transition as a function of the Reynolds number to the junction of the hemisphere-cylinder.